Dielectrophoretic manipulation of ribosomal RNA

Gerard Giraud,[1,a)] Ronald Pethig,[2] Holger Schulze,[3] Grace Henihan,[3] Jonathan G. Terry,[2] Anoop Menachery,[2] Ilenia Ciani,[4] Damion Corrigan,[4] Colin J. Campbell,[3] Andrew R. Mount,[4] Peter Ghazal,[3] Anthony J. Walton,[2] Jason Crain,[1,5] and Till T. Bachmann[3,b)]
[1]*School of Physics and Astronomy, University of Edinburgh, Edinburgh EH9 3JZ, United Kingdom*
[2]*Institute for Integrated Micro and Nano Systems, School of Engineering, University of Edinburgh, Edinburgh EH9 3JF, United Kingdom*
[3]*Division of Pathway Medicine, College of Medicine and Veterinary Medicine, University of Edinburgh, Edinburgh EH16 4SB, United Kingdom*
[4]*School of Chemistry, University of Edinburgh, Edinburgh EH9 3JJ, United Kingdom*
[5]*National Physical Laboratory, Teddington TW11 0LW, United Kingdom*

(Received 11 March 2011; accepted 6 June 2011; published online 28 June 2011)

The manipulation of ribosomal RNA (rRNA) extracted from *E. coli* cells by dielectrophoresis (DEP) has been demonstrated over the range of 3 kHz–50 MHz using interdigitated microelectrodes. Quantitative measurement using total internal reflection fluorescence microscopy of the time dependent collection indicated a positive DEP response characterized by a plateau between 3 kHz and 1 MHz followed by a decrease in response at higher frequencies. Negative DEP was observed above 9 MHz. The positive DEP response below 1 MHz is described by the Clausius–Mossotti model and corresponds to an induced dipole moment of 3300 D with a polarizability of 7.8×10^{-32} F m^2. The negative DEP response above 9 MHz indicates that the rRNA molecules exhibit a net moment of −250 D, to give an effective permittivity value of 78.5 ε_0, close to that of the aqueous suspending medium, and a relatively small surface conductance value of ~0.1 nS. This suggests that our rRNA samples have a fairly open structure accessible to the surrounding water molecules, with counterions strongly bound to the charged phosphate groups in the rRNA backbone. These results are the first demonstration of DEP for fast capture and release of rRNA units, opening new opportunities for rRNA-based biosensing devices. © *2011 American Institute of Physics.* [doi:10.1063/1.3604395]

I. INTRODUCTION

The RNA molecule is a linear polymer in which nucleotides are linked by phosphodiester units. The molecule carries negative charges along its backbone associated with ionized phosphate groups, and in aqueous solutions these charges are screened by counterions. Generally RNA has regions which are self-complementary (A-U or G-C pairing) leading to the presence of loops and folded motifs. Ribosomes consist of RNA subunits (such as the 16S and 23S subunit studied here) which translate mRNA into polypeptides during protein synthesis. All living organisms contain ribosomal RNA (rRNA). Consequently, rRNA has been used for evolutionary science and taxonomy and utilized to define and identify different organism species.[1,2] The high copy numbers of rRNA molecules present in individual cells have also been used as a naturally amplified biomarker for the detection of bacteria in proof of concept, environmental and clinical studies.[3–5] The integration of such techniques in modern bioanalytical devices such as micro total analysis systems

a)Author to whom correspondence should be addressed. Electronic mail: gerard.giraud@ed.ac.uk
b)Electronic mail: till.bachmann@ed.ac.uk

(μTAS) and point of care testing[6] (POCT) requires advances in minimally invasive technology to enable efficient concentration, trapping and separation of RNA molecules.

Dielectrophoresis (hereafter DEP) is a contact-free manipulation technique based on the induced motion of polar or polarizable particles (with or without charges) in a nonuniform electric field.[7–9] The technique has been used to characterize and manipulate a number of biological particles ranging from micrometer-size cells and bacteria to spores and viruses of nanometer dimensions.[10–12] The latest development of the technique and the scope of its applications have been recently compiled in two comprehensive reviews.[9,13]

The work presented here demonstrates for the first time the DEP collection and repulsion of 16S and 23S subunits of *E. coli* rRNA using microelectrodes. The DEP responses were measured as a function of the strength and frequency of an applied non-uniform electric field. Using microfabricated interdigitated electrodes (IDEs) and the total internal reflection fluorescence (TIRF) microscopy technique, we were able to observe that rRNA subunits exhibited both positive and negative DEPs.

Although the DEP properties of RNA have not been reported previously, pertinent dielectric studies of the free RNA subunit of 70S rRNA have been performed and interpreted to indicate that counterion fluctuations dominate the dielectric dispersions centered around 9 MHz at 25 °C.[14] Also of relevance are the DEP studies performed for a variety of DNA systems,[15,16] spanning micron-sized plasmids[17] to short-stranded single molecule DNA.[18] The positive DEP response of DNA is found to decrease with increasing frequency,[17,18] consistent with the reduction in effective polarizability measured by dielectric spectroscopy.[19] However, the transition from a positive to a negative DEP response has only been reported for micrometer-size λ-DNA.[20,21] Electric dichroism measurements on transfer RNA (tRNA) indicate that they have permanent dipole moments of $\sim 10^{-27}$ C m ($\sim$300 D) associated with the asymmetric distribution of phosphate charges with respect to the center diffusion.[22] To our knowledge, a value for the permanent dipole moment of either the 16S or 23S subunit of rRNA has not been evaluated, but because of their asymmetric tertiary structures we can expect them to possess permanent moments. The secondary structure (helices, loops, and bulges) of the rRNA molecule can be expected to remain intact at room temperature at the low ionic concentrations ($\sim$1 mM) used in our DEP experiments, but aspects of the tertiary structure can be expected to be lost as a result of the reduced screening of the charged phosphate groups.[23] Our finding reported here of a transition from a positive to a negative DEP response for rRNA provides the means to examine more thoroughly the relative contributions that the permanent dipole moment, counterion fluctuations, and motions of the molecular structure make to the DEP response of nucleic acid polymers.

II. THEORY

A. Dielectrophoretic force

A DEP force arises when an electrically polar or polarizable particle experiences a nonuniform electric field. The direction in which the force acts depends on the frequency of the applied field and on the difference between the polarization properties of the particle and the surrounding medium. Solvated particles can respond to this force by moving either up (positive DEP) or down (negative DEP) the field gradient. As a result, observation of the positive and negative regimes and the DEP crossover point is useful not only as a manipulation tool but also as a means of elucidating the frequency dependence of the different contributions to the polarization.

The DEP force acting on a dipole of moment m in a field gradient is given by

$$F_{\mathrm{DEP}} = m \nabla E, \tag{1}$$

where ∇ represents the gradient operator acting on the applied field E. In the most general case, the dipole moment m will be composed of a permanent dipole moment m_p and an induced moment m_{ind}, such that

$$m = m_p + m_{\text{ind}} = m_p + \rho \nu E, \tag{2}$$

in which ν is the volume of the polarizable particle and ρ is the polarizability per unit volume.

From Eqs. (1) and (2), and for a conservative and irrotational field:

$$F_{\text{DEP}} = (m_p + \rho \nu E) \nabla E = m_p \nabla E + \tfrac{1}{2} \rho v \nabla E^2. \tag{3}$$

The results shown in Fig. 4 (inset) of the DEP voltage dependence measured at 1 MHz reveal that a quadratic relationship is dominant, which from Eq. (3) indicates that any contribution of the permanent dipole moment m_{p} to the DEP of rRNA is minimal at 1 MHz.

We will assume that the rRNA molecules maintain their secondary structures, as well as some aspects of their tertiary structures, so that as a first approximation they can be treated as spherical particles of radius R. On the assumption that the permanent moments of the rRNA molecules do not significantly influence the DEP response, the time-dependent average expression for the DEP force acting on them is given by[7]

$$\langle F_{\text{DEP}} \rangle = 2\pi \varepsilon_o \varepsilon_m R^3 \, \text{Re}[f(\varepsilon^*)] \nabla E^2. \tag{4}$$

In Eq. (4), E is the root-mean-square amplitude of the applied nonuniform ac field, $\varepsilon_o \varepsilon_m$ is the absolute permittivity of the suspending medium, and $f(\varepsilon^*)$ is the Clausius–Mossotti factor given by[8]

$$f(\varepsilon^*) = \left(\frac{\varepsilon_p^* - \varepsilon_m^*}{3(\varepsilon_m^* + A(\varepsilon_p^* - \varepsilon_m^*))} \right). \tag{5}$$

In this equation, the complex permittivity of the particle and suspending medium are given as $\varepsilon_i^* = \varepsilon_o \varepsilon_i - j\sigma_i / \omega$ in which ω is the radian frequency (2πf) of the applied field, and $j = \sqrt{-1}$. The subscript i denotes either the particle (p) or the medium (m). In the case of a spherical particle, the depolarization factor A = 1/3 leading to $f(\varepsilon^*) = (\varepsilon_p^* - \varepsilon_m^*)/(\varepsilon_p^* + 2\varepsilon_m^*)$.

In the frequency range of our investigation (10^3–10^7 Hz), we assume that the induced dipole moment $m(\omega)$

$$m(\omega) = 4\pi \varepsilon_o \varepsilon_m R^3 \, \text{Re}[f(\varepsilon^*)] E \tag{6}$$

is primarily due to the reorganization of interfacial charges between the particle and the solvent, namely, surface conductivity and field-induced diffusion of counterions in the electrical double layer around the particle.

$\text{Re}[f(\varepsilon^*)]$ can then be written in the form[24]

$$\text{Re}[f(\varepsilon^*)] = \frac{\varepsilon_o \varepsilon_m}{1 + \omega^2 \tau^2} \left[\omega^2 \tau^2 \left(\frac{\varepsilon_p - \varepsilon_m}{\varepsilon_p + 2\varepsilon_m} \right) + \left(\frac{\sigma_p - \sigma_m}{\sigma_p + 2\sigma_m} \right) \right], \tag{7}$$

where the interfacial polarization relaxation time τ is given by[25]

$$\tau = \frac{\varepsilon_p + 2\varepsilon_m}{\sigma_p + 2\sigma_m} \varepsilon_o. \tag{8}$$

Equation (7) simplifies to show that the frequency dependence of interfacial charges is dominated by conductivity at low frequency and permittivity at high frequency.

$$\mathrm{Re}[f(\varepsilon^*)]/\varepsilon_m\varepsilon_0 = \begin{cases} \dfrac{\sigma_p - \sigma_m}{\sigma_p + 2\sigma_m} & \text{for } \omega\tau \ll 1 \\ \dfrac{\varepsilon_p - \varepsilon_m}{\varepsilon_p + 2\varepsilon_m} & \text{for } \omega\tau \gg 1. \end{cases} \tag{9}$$

Positive DEP occurs for $\mathrm{Re}[f(\varepsilon^*)]>0$, leading to accumulation of particles at the electrode edges in region of high electric field. Conversely for $\mathrm{Re}[f(\varepsilon^*)]<0$, the particles are repelled from the electrode edge in the direction of regions of decreasing field strength.

In Eqs. (5) and (7), the values of the particle and medium conductivity and permittivity are assumed to remain constant as a function of frequency. Dielectric measurements on RNA and DNA suspensions[14,15,17] indicate that dispersions associated with conformational relaxations of the molecular structure occur in the frequency range of relevance to our studies reported here. To accommodate the possibility that such dispersions might influence the DEP response of RNA, we have introduced a frequency dependence of the particle permittivity and conductivity according to the Debye equation:

$$\varepsilon_p^* = \varepsilon_\infty + \frac{\varepsilon_s - \varepsilon_\infty}{1 + j\omega\tau_d}, \tag{10}$$

where ε_∞ is the permittivity at the high frequency limit of the dispersion, ε_s is the low frequency limiting permittivity, and τ_d is the characteristic dipolar relaxation time. This complex permittivity can be decomposed into real and imaginary parts as

$$\varepsilon_p'(\omega) = \varepsilon_\infty + \frac{\varepsilon_s - \varepsilon_\infty}{1 + (\omega\tau_d)^2}, \tag{11}$$

$$\varepsilon_p''(\omega) = \frac{(\varepsilon_s - \varepsilon_\infty)\omega\tau_d}{1 + (\omega\tau_d)^2}. \tag{12}$$

The dielectric loss parameter $\varepsilon_p''(\omega)$ gives rise to a particle conductivity term $\sigma_p(\omega)=\omega\varepsilon_p''(\omega)$. To account for the mobility of counterions in the electrical double layer surrounding the RNA molecule, we assign a surface conductance K_s to be added to the particle bulk conductivity σ_b.[9,17] The particle conductivity is thus composed of three terms given by

$$\sigma_p = \sigma_b + \frac{2K_s}{R} + \omega\varepsilon_p''(\omega). \tag{13}$$

B. Finite element method simulation

Finite element simulations (COMSOL MULTIPHYSICS) were used to compute the electric field (dc voltage) generated in three dimensions on the gold interdigitated electrode (IDE) arrays. The DEP force is proportional to the gradient of the squared electric field, ∇E^2, and this factor is plotted Fig. 1 by considering a voltage of 2 V (peak) between the electrodes and a value of the relative permittivity of water $\varepsilon_m=80.2$. The factor ∇E^2 is minimal in the middle of the gap between electrodes and reaches a maximum at the edge of the electrode finger with a value greater than of 10^{19} $\mathrm{V^2/m^3}$. Figure 1(a) shows that the DEP force extends above the electrode, but with decreasing strength. At 20 μm above the electrode surface, the factor ∇E^2, and hence the DEP force, has decreased by two orders of magnitude.

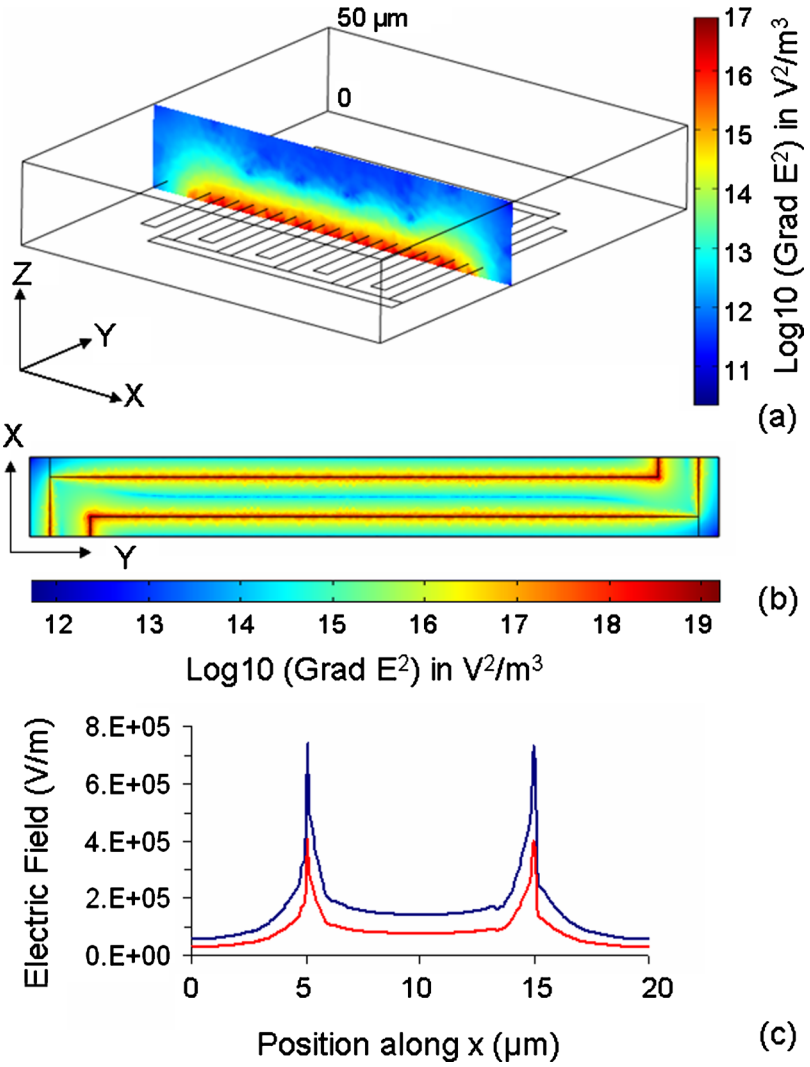

FIG. 1. (a) Contour plot of the gradient of the squared field, ∇E^2, generated across the gold IDE, up to 50 μm above the electrode's surface. (b) Contour plot of ∇E^2, simulated in the plane between two fingers separated by 10 μm. The DEP force is minimal in the middle of the gap and reaches a maximum value at the edge of the electrode's finger. The voltage between the electrodes is 2 V (peak). (c) Electric field cross section between two electrode fingers calculated for an applied voltage of 1.1 V (peak) (red) and 2 V (peak) (blue).

III. MATERIAL AND METHODS

A. Experimental setup

Live monitoring of the rRNA dielectrophoretic activity was performed using the setup depicted in Fig. 2. Our customized flow cell (Ref. 26) of total internal volume 900 μl was first cleaned with RNAaseZap (Ambion, Warrington, UK), washed thoroughly with pure water and rinsed with methanol. This treatment prevented sample degradation through contamination during the experiment. The array of interdigitated electrodes ("IDE chip") was cleaned with Piranha solution (3:1 ratio of concentrated sulfuric acid mixed with hydrogen peroxide solution [30% (w/w) in H_2O; Sigma Aldrich, UK]) for 10 s, washed with water, dried under nitrogen flow, and placed into the flow cell.

Figure 2 (inset) shows a photograph of a single gold IDE produced by microfabrication technique (Ref. 26). The RiboGreen-labeled rRNA sample was then injected into the cell and positioned on the stage of a TE300 Nikon inverted microscope. An excitation beam at 455 nm was

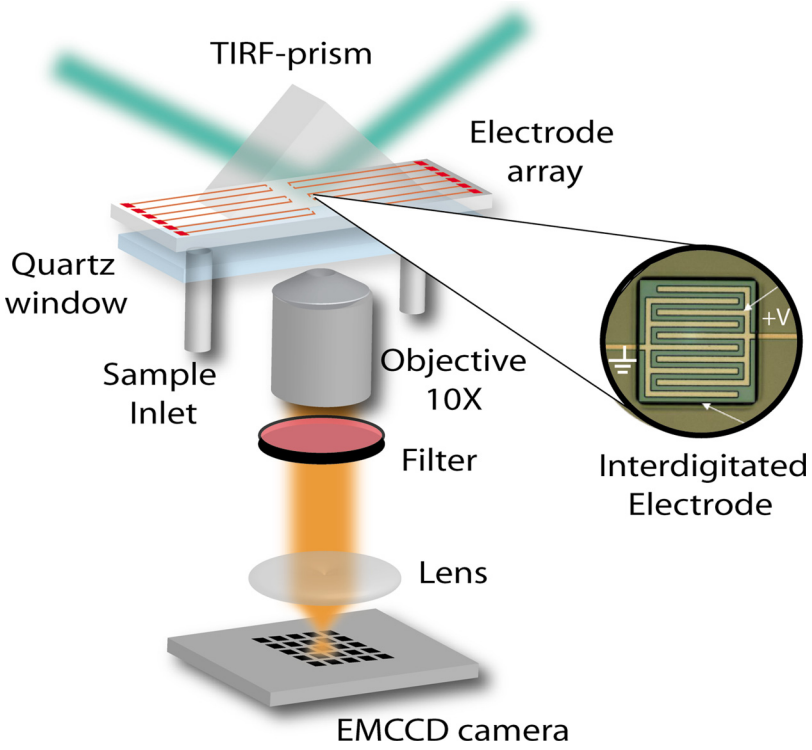

FIG. 2. Experimental setup for live monitoring of rRNA dielectrophoretic activity. The IDE chip positioned into a flow cell is excited by prism based evanescent wave. Fluorescence images of RiboGreen-labeled rRNA are collected with a 10× objective and imaged on an EMCCD camera. The zoom shows a plan view of a 200 μm^2 gold IDE with 10 μm electrode fingers and 10 μm gap.

produced by frequency doubling the output beam of a femtosecond Ti:sapphire laser system (10 W Verdi and Mira from Coherent, Glasgow, Scotland) and directed to excite the sample on the IDE chip by total internal reflection. In order to achieve this, a quartz prism (Cairn Research, Faversham, UK) was attached to the microscope's condenser and placed into contact with the undersurface of the chip using transmission immersion oil. The laser beam was directed below critical angle and focused onto the IDE chip, generating a local evanescent excitation of approximately 1 mm^2 area with an average power of 1 mW. The resulting fluorescence was then collected with a plan apo Nikon X10 objective, filtered with an emission band pass filter (535/50 nm) and imaged onto an Electron Multiplying Charge Coupled Device (EMCCD) Camera (Ixon, Andor, Belfast, UK) synchronized to an external Shutter (Oriel, Didcot, UK). AC voltage between 3 kHz and 50 MHz was delivered by a pulse generator (HP, 50 MHz, 8112A). Finally, DEP movies were obtained by capturing one 256×256 pixel frame every 2 s for 60 s.

B. Sample preparation

Escherichia coli (E. coli) DH10β was cultivated using an overnight culture of 2 ml Luria-Bertani (LB) medium (Sigma Aldrich, UK) containing 10 g/l Bacto-tryptone, 5 g/l yeast extract, and 10 g/l NaCl. The medium was inoculated with an *E. coli* colony from a LB agar plate and incubated for 16 h at 37 °C in a shaking incubator. Total RNA was isolated with RNeasy Protect Bacteria Mini Kit (Qiagen, Hilden, Germany), using proteinase K and β-mercaptoethanol treatment to remove protein and on-column DNase treatment was performed to remove genomic DNA. The *E. coli* culture was mixed with RNAprotect Bacteria Reagent solution prior cell lysis according to the protocol provided by the manufacturer. This patent-pending solution stabilizes RNA before cell lysis and prevents RNA degradation. The extracted nucleic acids were then eluted into 30 μl of distilled DNase and RNase free water (GIBCO, Invitrogen, Paisley, UK). All rRNA

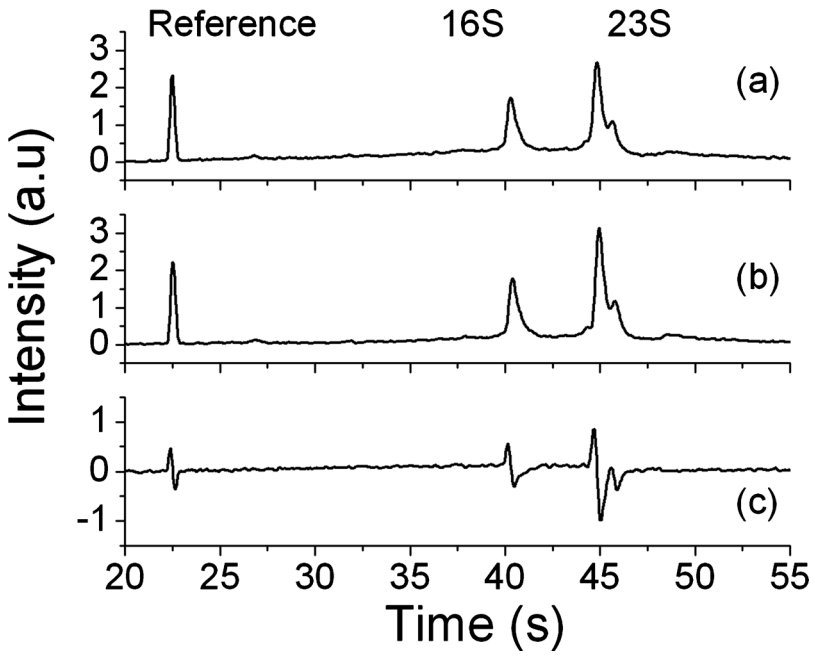

FIG. 3. Electropherograms of the rRNA sample measured (a) before DEP and (b) after a duration of 6 h, during which time multiple series of DEP measurements took place. (c) shows the difference spectrum [(a) and (b)].

solutions for DEP experiments were prepared with distilled DNase and RNase free water. The sample contains all RNA over 200 nt and subsequent gel electrophoresis confirmed the presence of the 16 S (1541 nt) and 23 S (2904 nt) rRNA.

The extracted sample was subsequently labeled with RiboGreen (Quant-iT™ RiboGreen® RNA Reagent, Invitrogen, UK). Typically, 2.5 μl of the dye was added to 1 ml of RNA (diluted in water at a given concentration). The sample was then left at RT for 5 min. The remaining free dye was then removed by size exclusion gel filtration using an Illustra MicroSpin G-50 Column, (GE Healthcare, UK).

Sample concentration was estimated by measuring the oligonucleotide absorption band at 260 nm of each sample after extraction using a Nanodrop absorbance spectrometer (Thermo Fisher Scientific, Wilmington, NC). A 30 μl sample with 700 ng/μl RNA was diluted in 870 μl leading to a final concentration of 24 ng/μl (38 nanomoles dm^{-3}) total RNA of which about 80% is ribosomal RNA.[27] The integrity of the sample was evaluated by microfluidics-based electrophoresis with an Agilent Bioanalyzer (Agilent, Wokingham, UK). Figure 3(a) shows the electropherograms after elution. The two sharp peaks correspond to the 16S and 23S subunits and present an amplitude ratio of 0.8.

C. DEP measurement and data analysis

Time dependent DEP measurements were performed on samples, prepared according to the methods described above, suspended in an aqueous medium of conductivity 13 mS/m as measured using an Oakton-510 conductivity meter (Oakton Instruments, Illinois). The DEP measurements were conducted for a range of voltage values and frequencies applied to the IDE, referred to as "voltage series" and "frequency series." For each series, a single IDE was used to record an average of 20 DEP collection cycles, corresponding to 20 DEP movies. This approach, which limits systematic variations between IDEs, required the removal of the RNA particles from the electrode between individual measurements. This was achieved by negative DEP by applying a 6 V ac field at 50 MHz to the IDE for 2 min.

After electrode cleaning, positive DEP was measured by recording the increase in fluorescence intensity observed on the IDE. It was also possible to monitor the decrease in fluorescence intensity on the electrode, corresponding to either the diffusion of the collected RNA particles away from the electrode edges (with electric field off) or as a result of negative DEP observed for field frequencies above 9 MHz. For the quantitative analysis of the data, the amount of rRNA collected on the IDE was obtained from each frame of the DEP movie by determining the mean fluorescence intensity after background subtraction inside the 200 μm^2 of the electrode area (120×120 pixels). The negative DEP response was much weaker than that obtained for positive DEP. Negative DEP collection data were therefore further processed by subtracting the voltage-independent diffusion of rRNA from the change in fluorescent intensity obtained with the field applied. This should have removed inclusion of any subtle effects arising from heat-induced fluid flow caused by the laser beam. The gain of the EMCCD camera was optimized for each sample and was maintained at this setting for three series of measurements, each performed on three individual IDEs, therefore allowing for direct comparison of the fluorescence absolute values.

IV. RESULTS

A. Sample stability

The integrity of the sample was evaluated by microfluidics-based electrophoresis with an Agilent Bioanalyzer. Figure 3 shows the electropherograms of the used ribosomal RNA sample before (a) and after DEP testing (b). The two sharp peaks of approximately equal amplitude correspond to the 16S and 23S subunits of the rRNA. The difference spectrum displayed in Fig. 3(c) reveals very little variations, demonstrating that the rRNA has remained intact after 6 h experimental manipulation.

B. Voltage dependence

The voltage dependence of the rRNA DEP collection was investigated by recording the DEP movies obtained on a single electrode biased with a series of applied voltage ranging from 0 to 5 $V_{p\text{-}p}$. Figure 4 shows the fluorescence intensity time traces obtained for 17 different voltages at 1 MHz frequency. The voltage dependence displayed in Fig. 4 (inset) reveals three distinct regimes. (i) Between 0 and 2.2 V, the signal intensity remains constant. In this range, the DEP force is too weak to overcome Brownian motion. (ii) From 2.2 to 3.8 V, the fluorescence signal is quadratic in applied electric field as expected according to Eq. (4). (iii) Above 3.8 V, the DEP signal still increases; however, its dependence is no longer quadratic. This effect was considered to arise from the number of collected RNA particles saturating the volume available to them in the space interrogated by the TIRF technique. The initial amount of RNA contained in the volume (1.1×10^{-11} dm^3) bounded by the TIRF depth of field (275 nm) and the IDE array (area 4×10^{-6} dm^2) was 4.2×10^{-19} moles. This is equivalent to 2.5×10^5 RNA particles, which occupy a total volume of $\sim 10^{-15}$ dm^3. From the increase in fluorescence intensity above the background observed for the DEP measurements between 1 kHz and 1 MHz, we estimate that a 10^3-fold increase in RNA concentration occurred after 30 s of an applied 4 $V_{p\text{-}p}$ signal. At this concentration within the "TIRF volume," mutual electrostatic repulsions between the charged rRNA molecules will begin to counterbalance the DEP force and result in the observed saturation of fluorescence.

The V^2-dependence of the fluorescence intensity rules out the possible influence on our DEP measurements of fluid flow arising from electrothermal effects because these exhibit a V^4-dependence.[28] Also, ac electro-osmosis, which does exhibit a V^2-dependence, peaks at a frequency several orders of magnitude smaller than the charge relaxation frequency ($\omega = \sigma/\varepsilon = 2.9$ MHz for our experiments) and falls off as a function of ω^2 thereafter.[28] Electro-osmosis is considered to exhibit a negligible influence on DEP, even for submicron-sized particles, above 100 kHz. We therefore consider that our observation of a V^2-dependence of fluorescence intensity reflects the DEP collection of our rRNA samples at the electrode edges, with negligible interference from induced fluid flow effects.

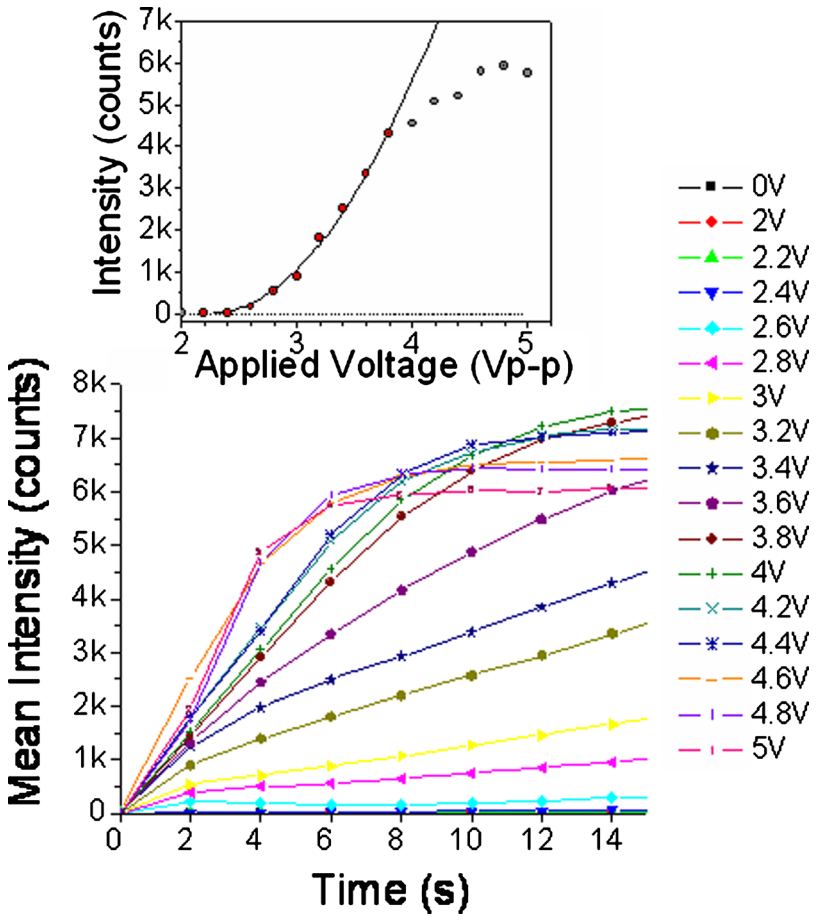

FIG. 4. DEP voltage dependence measured at 1 MHz. Intensity time traces obtained from 0 to 5 $V_{p\text{-}p}$. In inset is shown the DEP voltage dependence plotted at 6 s after the onset of DEP, along with the quadratic function F (line) given by the equation $F=A(V-V_{min})^2$ with $A=1774$ and $V_{min}=2.23$. The quadratic dependence of the DEP is observed between $V_{p\text{-}p}=2.2$ and 3.8 V.

C. Frequency dependence

The frequency dependence of the rRNA DEP collection was investigated in a range spanning from 3 kHz to 50 MHz. This was done by applying a 4 V_{p-p} AC field to the electrode at a given frequency for 60 s. Figure 5 shows a series of typical images captured at 4, 10, and 30 s after the onset of DEP and obtained for an IDE with an applied field frequency of 100 kHz [Fig. 5(a) (enhanced)], 3 MHz [Fig. 5(b) (enhanced)], and 50 MHz [Fig. 5(c) (enhanced)] (50 MHz measured after positive DEP at 100 kHz). The signal integration of such DEP movies resulted in a series of time traces. Figure 6(a) shows the intensity time traces obtained for nine frequencies, averaged over three individual electrodes.

The DEP collection time profiles present two regimes. At time t shorter than the transition time $T_{transition}$, the intensity signal rises linearly. In this regime, referred to as *the initial collection rate*, the particles collect under the action of the DEP force alone. For $t>T_{transition}$, the collection of particles reaches a steady state regime. As shown in Fig. 6(a), $T_{transition}$ increases with increasing frequencies. These observations are consistent with the DEP of micrometer-size DNA plasmids for which similar time behaviors have been reported.[17]

The collection rate was evaluated by calculating the slope $(\partial I/\partial t)$ of each time trace. This was done by considering the first 10–15 s of DEP where the signal increase is linear. The collection rate frequency dependence is shown Fig. 6(b). Between 3 kHz and 1 MHz, the collection effi-

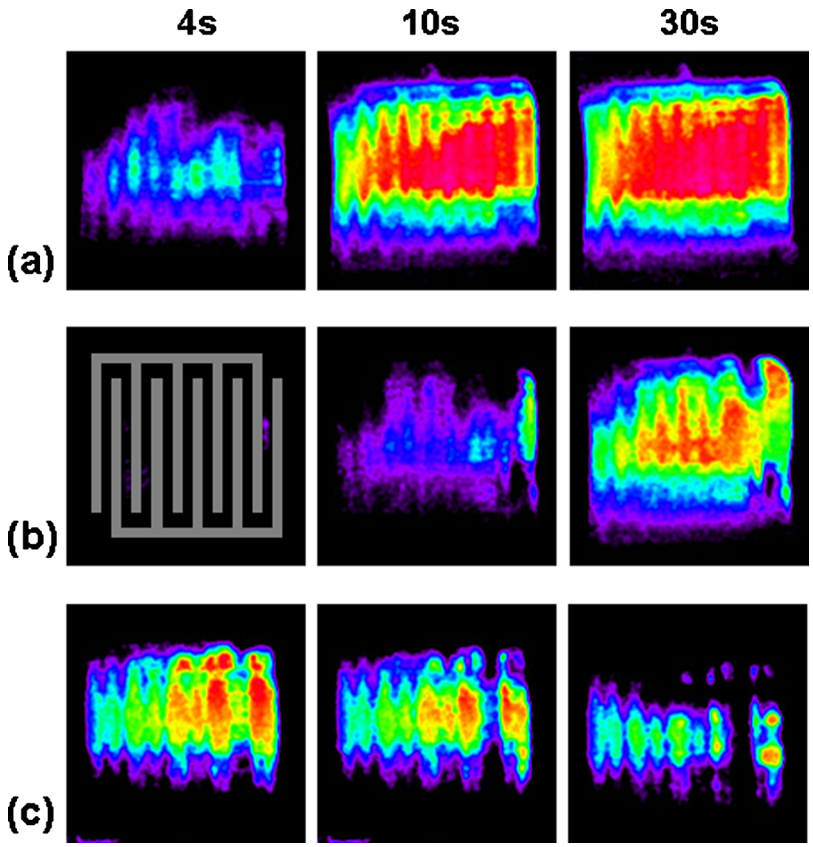

FIG. 5. Color coded TIRF images extracted from rRNA DEP movies at 4, 10, and 30 s after the onset of a 4 $V_{p\text{-}p}$ ac field set at: (a) 100 kHz, (b) 3 MHz, and (c) 50 MHz measured after positive DEP at 100 kHz. Image processing included background subtraction and Gaussian smoothing. An outline of the electrode is superimposed on the first image of the 3 MHz series (enhanced online).
[URL: http://dx.doi.org/10.1063/1.3604395.1]
[URL: http://dx.doi.org/10.1063/1.3604395.2]
[URL: http://dx.doi.org/10.1063/1.3604395.3]

ciency remains constant with an average value of 900 counts/s. At frequency higher than 1 MHz, the collection efficiency drops sharply, down to zero in the region of 9 MHz, defined as the cross over frequency. At higher frequencies, negative DEP is observed.

V. ANALYSIS AND DISCUSSION

The results shown in Fig. 4 (inset) of the DEP voltage dependence measured at 1 MHz reveal that a quadratic dependence is dominant, which indicates that any contribution of a permanent dipole moment (which would be revealed as a linear dependence on voltage) to the DEP of rRNA is minimal at 1 MHz. The negative DEP response above 9 MHz also suggests that the induced dipole moment reverses polarity at high frequencies, with the Clausius–Mossotti factor of Eq. (5) assuming a negative value. Our procedure for evaluating the frequency dependence of the DEP response of rRNA is thus to neglect a possible contribution from the permanent dipole moment. Our analysis follows two possible models. The first assumes that the conventional Clausius–Mossotti model is relevant and that the induced dipole moment $m(\omega)$ primarily arises from the reorganization of interfacial charges between the particle and the solvent, and includes a surface conductivity associated with field-induced diffusion of counterions in the electrical double layer around the particle. The second model takes into account dispersion effects resulting from the

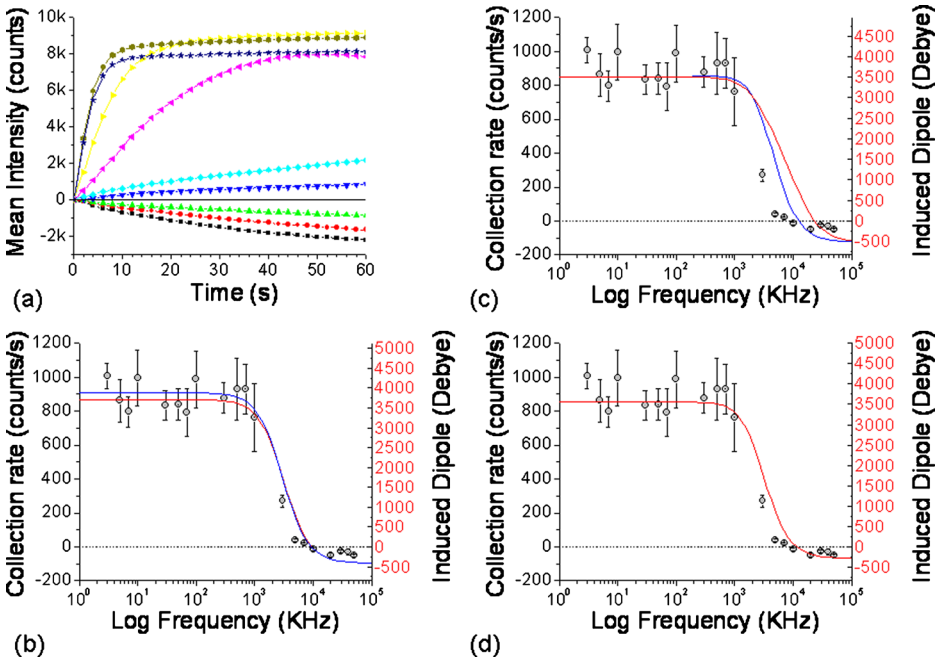

FIG. 6. (a) DEP collection time profiles obtained at 4Vpp (from top to bottom) at 10 kHz (brown), 100 kHz (blue star), 1 MHz (yellow), 3 MHz (pink), 5 MHz (light blue), 7 MHz (blue triangle), 10 MHz (green), 30 MHz (red), and 50 MHz (black). (b) Collection rate frequency dependence measured from 3 kHz to 50 MHz. Standard deviation was calculated over three "frequency series" measurements, performed on three different electrodes. The solid lines correspond to the Clausius–Mossotti model calculated with the parameters presented in Table I and assuming either spherical rRNA (red curve), with depolarization factor $A=1/3$ or stretched rRNA (blue curve) with $A=0.1$, corresponding to a prolate ellipsoid of ratio 3:1 for the major and minor axes. (c) corresponds to the Clausius–Mossotti model with dispersion parameters $\varepsilon_s=108\ \varepsilon_0$ and $\varepsilon_\infty=78\ \varepsilon_0$ obtained from Ref. 14, $K_s=0.15$ nS and $f_{xo}=1$ MHz (blue curve) or $f_{xo}=9$ MHz (red curve). In both cases, the rRNA is considered to be spherical (A=1/3). (d) corresponds to the Clausius–Mossotti model with parameters $\varepsilon_s=83\ \varepsilon_0$, $\varepsilon_\infty=77\ \varepsilon_0$, $K_s=0.1$ nS, and $f_{xo}=1$ MHz. In this case, rRNA is considered elliptical with a ratio of 3:1 for the major and minor axes, corresponding to a depolarization factor A=0.1

intrinsic dipolar fluctuations of the particle's molecular structure. In both cases the effect of a possible field-induced elongation, and thus a departure from an overall spherical configuration, of the rRNA molecules is also taken into account.

A. Data normalization: rRNA polarizability

The DEP collection rate $\partial I/\partial t$ is related to the DEP force, which in turn is proportional to the real part of the induced dipole moment Re(m) calculated according to Eq. (6). The DEP collection rate and induced dipole can be normalized by considering the energy of a particle when the deterministic DEP force exactly counteracts the stochastic Brownian force. The total particle energy U_{tot}, expressed as the sum of a thermal kinetic energy U_{th} associated with Brownian motion, and an attractive potential energy U_{DEP} associated with DEP, is zero according to[18]

$$U_{\text{tot}} = U_{\text{th}} + U_{\text{DEP}} = \frac{3}{2}k_B T + \frac{1}{2}\alpha E_{\text{min}}^2 = 0, \tag{14}$$

where k_B is the Boltzmann constant and α is the rRNA polarizability. The minimum voltage to trap rRNA at the electrodes, as determined from the DEP voltage dependence at 1 MHz [see Fig. 4 (inset)], is estimated as $V_{\text{min}}=2.2\ V_{\text{p-p}}$, corresponding to a minimum electric field $E_{\text{min}}=4.10^5$ V/m [calculated at the edge of the electrode (Fig. 1(c)]. From Ref. 18, we obtain a rRNA polarizability $\alpha=3k_BT/E_{\text{min}}^2=7.8\times10^{-32}$ F m^2. This value is of the same order as polarizability obtained for DNA plasmids pUC18 (2700 bp) with $\alpha=1\times10^{-32}$ F m^2 (Ref. 29) and pBVboostFG

TABLE I. List of the parameters used in the Clausius–Mossotti model.

Definition	Symbol	Values	Details
Suspending medium permittivity	ε_m	80.2 ε_0	From Ref. 31
Suspending medium conductivity	σ_m	0.013 S/m	Measured
Applied ac field (peak)	E	200 kV/m	Measured
Particle radius (rRNA)	R	10 nm	From Ref. 30
rRNA effective conductivity	σ_P	0.015 ± 0.002 S/m	Calculated according to the system of Eq. (18)
rRNA absolute permittivity	ε_P	78.5 ± 1.5 ε_0	with $\omega_I = 1.8 \pm 0.1$ MHz and $\omega_X = 9$ MHz
rRNA induced dipole moment at 1 MHz	μ_{RNA}	3297 D	Calculated according to Eq. (14)

(1065 bp) with $\alpha = 8.5 \times 10^{-32}$ F m^2.[18] The average induced dipole moment of our rRNA at 1 MHz and 4 $V_{p\text{-}p}$ (1.4 V_{rms}) can thus be calculated as $m = \alpha E = 1.1 \times 10^{-26}$ C m (equivalent to 3297 D). This value was used to normalize the DEP collection rates with the Clausius–Mossotti functions shown in Figs. 6(b)–6(d).

B. Clausius–Mossotti model

The conventional Clausius–Mossotti model, as described in Sec. II, was utilized to represent the frequency dependent DEP data presented in Fig. 6(b) using the parameters listed in Tables I and II. The conductivity of the medium was measured and its permittivity obtained from the literature. The radius of the 23S rRNA particle was extracted from the crystal structure of the complete 70S ribosome[30] and estimated at 10 nm. Considering that the samples contained both the 16S and 23S subunits, this value should be considered as an upper estimate. The effective conductivity and permittivity of rRNA were calculated by analyzing the frequency dependent collection rate of the particle in terms of the induced dipole moment and the DEP force of the molecule.

The results of Fig. 6(b) indicate that the rRNA molecules exhibit positive DEP at low frequencies and negative DEP above 9 MHz, which from Eq. (9) imply that $\sigma_p > \sigma_m$ and $\varepsilon_p < \varepsilon_m$. The conductivity σ_m of the aqueous suspending medium was measured to be 12.8 mS/m, and we can assume a value $\varepsilon_m \approx 80.2$ for the relative permittivity of the medium (water at 20 °C).[31] At the cross-over frequency f_{xo}, the induced dipole moment is zero, which implies that $\mathrm{Re}[f(\varepsilon^*)]$ in Eq. (2) is null. From Eqs. (7) and (8), the following quadratic expression that satisfies this condition can be derived:

$$\omega_{xo}^2 = \frac{1}{(\varepsilon_o)^2} \frac{(\sigma_m - \sigma_p)(\sigma_p + 2\sigma_m)}{(\varepsilon_p - \varepsilon_m)(\varepsilon_p + 2\varepsilon_m)}. \tag{15}$$

A valid (i.e., real) value for the cross-over frequency f_{xo} exists for the situation $(\sigma_m - \sigma_p)/(\varepsilon_p - \varepsilon_m) > 0$, and the relationships $\sigma_p > \sigma_m$ and $\varepsilon_p < \varepsilon_m$ derived from the experimental results satisfy this condition.

The DEP force varies with frequency as

TABLE II. List of the parameters used in the Clausius–Mossotti model including dispersion.

Definition	Symbol	Values
rRNA depolarization factor	A	0.1 ± 0.01
rRNA surface conductance	K_S	0.1 ± 0.01 nS
rRNA high frequency permittivity	ε_∞	77 ± 1 ε_0
rRNA low frequency permittivity	ε_S	83 ± 1 ε_0

$$F_{\mathrm{DEP}}(\omega) = F_{\mathrm{DEP}}(\infty) + \frac{F_{\mathrm{DEP}}(0) - F_{\mathrm{DEP}}(\infty)}{1 + \omega^2\tau^2}, \tag{16}$$

where $F_{\mathrm{DEP}}(0)$ and $F_{\mathrm{DEP}}(\infty)$ are the DEP forces at the low and high frequency limits, respectively.[32] At the inflection frequency ω_I, the second derivative of the DEP force vanishes:

$$\frac{\partial^2 F_{\mathrm{DEP}}(\omega)}{\partial^2 \omega} = \frac{2(F_{\mathrm{DEP}}(\infty) - F_{\mathrm{DEP}}(0))\tau^2(3\omega^2\tau^2 - 1)}{(1 + \omega^2\tau^2)^3} = 0. \tag{17}$$

The set of equalities in Eqs. (15) and (17) constitute a system of two equations with two unknowns:

$$\omega_{xo}^2 = \frac{1}{(\varepsilon_o)^2}\frac{(\sigma_m - \sigma_p)(\sigma_p + 2\sigma_m)}{(\varepsilon_p - \varepsilon_m)(\varepsilon_p + 2\varepsilon_m)},$$

$$\omega_I^2 = \frac{1}{3\tau^2}. \tag{18}$$

The inflection frequency ω_I and the cross-over frequencies, ω_{xo}, can be used to determine the values of the particle conductivity and polarizability by solving the system of equations (18). According to Fig. 6(b), ω_I and ω_{xo} were estimated to be 1.8 ± 0.1 and 9 MHz, respectively. Solving Eq. (18), σ_p and ε_p are calculated to be 0.015 ± 0.002 S/m and 78.5 ± 1.5 ε_0, corresponding to a polarization relaxation time of 51.6 ns calculated according to Eq. (8).

The fit of the experimental data to the Clausius–Mossotti model using the parameters listed in Table I is shown in Fig. 6(b). The red curve corresponds to a spherical molecular configuration with a depolarization factor $A = 1/3$. The blue curve shows the result obtained when considering a stretched molecule with a longitudinal/transversal ratio equal to 3:1. Both curves describe the positive DEP region rather well; however, the description relative to the negative part of the signal is less convincing.

The Clausius–Mossotti model can be further refined by introducing the frequency dependence of the particle permittivity and conductivity. In this case, the permittivity of rRNA is described by the high and low frequency permittivity parameters: ε_∞ and ε_s. Previous dielectric studies of rRNA (Ref. 14) reported values for ε_∞ and ε_s equal to 78 ε_0 and 108 ε_0, respectively. Figure 6(c) shows the theoretical curves obtained using these values with a cross-over frequency of 9 MHz in red and 1 MHz in blue. It is apparent that none of these curves represents the data satisfactorily. A more convincing representation is obtained when introducing a stretched molecular shape while decreasing the high permittivity parameter, as shown in Fig. 6(d).

C. rRNA: permittivity, conductivity, and molecular shape

The result of the analyses presented in Fig. 6(b) provides an estimate of the frequency dependent induced dipole moment of the rRNA particles. The rRNA permittivity value 78.5 ε_0 is close to the permittivity of the medium, suggesting that the rRNA is a fairly open structure which the solvent can penetrate. This could result from the negative charges of the phosphate backbone tending to repel each other and leading to an open structure. The effective particle conductivity σ_p for the model used in Fig. 6(b) is given by the sum of the particle's bulk conductivity σ_b and a surface conductivity expressed as

$$\sigma_p = \sigma_b + \frac{2K_s}{R}, \tag{19}$$

where K_s is a surface conductance whose magnitude depends on the composition and thickness of the electrical double layer surrounding the particle.[33] For a charged particle in a symmetrical ionic solution such as NaCl, the Debye screening length λ_D is given by

$$\lambda_D = (\varepsilon_o \varepsilon_m \bar{R} T / 2F^2 c)^{1/2}, \tag{20}$$

where $\bar{R}$ is the gas constant (8.314 J K^{-1} mol^{-1}), T is the absolute temperature, F is the Faraday constant (9.648×10^4 C mol^{-1}), and c is the concentration of ions in the solution (mol m^{-3}).[33] Assuming that NaCl is the dominant ionic salt remaining in the extracted sample, and noting that the equivalent ionic conductivity of NaCl is of the order 1.3×10^{-2} m^2 S mol^{-1} for a concentration in the range 0.5–10 mM,[31] then a measured value of 12.8 mS/m for the conductivity of the solution leads to an estimate of ~1 mol m^{-3} (i.e., ~1 mM) for the value of the concentration c in Eq. (20). From Eq. (20), the Debye screening length λ_D can thus be estimated to be ~10 nm, which is similar to the radius of the rRNA particle. This implies that the surface conductance K_s will have contributions arising from charge movements in both the Stern layer and the diffuse part of the double layer.[33] Solving Eq. (19) with σ_b equal to zero implies that in the case of rRNA, K_s cannot exceed 0.15 nS. This value is an order of magnitude smaller than the surface conductivity of a latex particle with a typical value of 1 nS.[34] The surface conductivity can be envisaged to take the form of an activated transport of the counterions, where the ions are thermally activated over potential energy barriers. The relatively small surface conductance obtained for the rRNA might therefore arise from a significant proportion of the counterions being strongly bound to the ionized phosphate groups and thus not freely delocalized over the whole molecular surface.

When combining dielectric dispersion effects and field-induced elongation of the rRNA, a better fit to the experimental data is obtained, as shown in Fig. 6(d). Stretching of oligonucleotides by DEP has been reported before in the case of DNA.[15,35] Considering the highly flexible nature of the rRNA molecules,[14] similar behavior might also be expected for our samples.

VI. CONCLUSIONS

This article has reported the DEP manipulation, over the frequency range from 3 kHz to 50 MHz, of a mixture of the 16S and 23S subunits of ribosomal RNA extracted from *E. coli*. To our knowledge, this is the first report of the DEP characterization of rRNA. The majority of DEP studies of DNA have reported[15,18] that DNA exhibits a positive DEP response that decreases in magnitude as the frequency of the applied nonuniform electric field enters the megahertz region. Some divergences exist regarding the DEP response at high frequency. One study[16] measured the capacitance changes observed between planar microelectrodes during DEP, revealing an increase for all DNA fragments ranging from 100 bp to 48 kbp, at frequency above 300 kHz. Another paper[21] investigating the DEP of micrometer-size lambda-DNA has in the contrary reported negative DEP above 10 MHz. Our finding that above 9 MHz rRNA makes the transition from positive to negative DEP is thus new to the study of the electrokinetic properties of nanometer-size polynucleic acids and opens up the possibility that rRNA samples can be condensed onto microelectrodes for physicochemical analysis or manipulation, and then released from the electrodes for further processing or analysis. It has recently been shown that DEP could be used in the megahertz regime to enhance hybridization efficiency.[36] This first demonstration of DEP for fast capture and release of rRNA subunits opens up new opportunities for rRNA-based biosensing devices.

The positive DEP response of rRNA below 1 MHz is well described by a model that assumes an induced dipole moment (as described by the classical Clausius–Mossotti theory) dominates over any effects associated with a permanent dipole moment. As discussed in the analysis of the DEP voltage dependence obtained at 1 MHz (Fig. 4), a linear dependence that would be indicative of a permanent dipole moment contribution is not evident. Furthermore, an analysis of the threshold voltage required for the DEP force to overcome Brownian motion [Eq. (14)] provides an estimate for the effective dipole moment of 1.1×10^{-26} C m (~3300 D), which is probably an order of magnitude larger than can be expected for the permanent dipole moment of RNA molecules.[22] The negative DEP response above 9 MHz indicates that the rRNA molecules exhibit a net moment of the order -8.3×10^{-28} C m (~−250 D). This moment could be composed of a positive permanent moment counteracted by a larger induced moment of opposite polarity. However, the negative DEP response is too weak to accurately determine a value for the threshold voltage for DEP and to confirm whether a linear voltage dependence (indicative of a permanent

moment) is imposed over a quadrature dependence. Further studies of the negative DEP response of rRNA are merited, if only to clarify the possible contribution of a permanent dipole moment.

Our DEP measurements and analyses have also provided estimates for the effective permittivity and conductivity of rRNA molecules. The value 78.5 ε_0 obtained for the effective permittivity of the RNA molecules is close to the permittivity of the aqueous medium. This suggests that rRNA has a fairly open structure accessible to the surrounding water molecules and could arise from mutual repulsion of the negative charges of the phosphate backbone. In dilute salt solutions, RNA has a partial (~50%) helical structure which results in a flexible polynucleotide structure.[23,37] However, our derived permittivity value could be an overestimate due to the neglect of a possible counteracting contribution to the DEP response of a permanent moment. From Eq. (9), we expect that the permittivity values of the particle and medium will dominate over their effective conductivities. The negative DEP response observed above 9 MHz is not insignificant, and this should lead to the expectation of deducing a permittivity value lower than 78.5 ε_0. This apparent inconsistency also merits further study regarding the magnitude of the permanent dipole moment of an rRNA molecule in dilute ionic solutions. Finally, the surface conductance value of ~0.1 nS is an order of magnitude smaller than that typically reported in the literature for small solid particles.[34] This could reflect the fact that the counterions are strongly bound to the charged phosphate groups in the RNA backbone, consistent with the finding that some 85% of the counterions are localized in tRNA.[22]

ACKNOWLEDGMENTS

This work was supported by Scottish Enterprise under the Chronic Wound Care program. Gerard Giraud, Ronald Pethig and Holger Schulze contributed equally to this study.

[1] S. G. Tringe and P. Hugenholtz, Curr. Opin. Microbiol. **11**, 442 (2008).
[2] S. Smit, J. Widmann, and R. Knight, Nucleic Acids Res. **35**, 3339 (2007).
[3] H. A. Joung, N. R. Lee, S. K. Lee, J. Ahn, Y. B. Shin, H. S. Choi, C. S. Lee, S. Kim, and M. G. Kim, Anal. Chim. Acta **630**, 168 (2008).
[4] J. Small, D. R. Call, F. J. Brockman, T. M. Straub, and D. P. Chandler, Appl. Environ. Microbiol. **67**, 4708 (2001).
[5] B. P. Nelson, T. E. Grimsrud, M. R. Liles, R. M. Goodman, and R. M. Corn, Anal. Chem. **73**, 1 (2001).
[6] H. Schulze, G. Giraud, J. Crain, and T. T. Bachmann, J. Biophoto. **2**, 199 (2009).
[7] D. Pohl, *The Behavior of Neutral Matter in Nonuniform Electric Fields* (Cambridge University Press, Cambridge, 1978).
[8] T. B. Jones, *Electromechanics of Particles* (Cambridge University Press, Cambridge, 1995).
[9] R. Pethig, Biomicrofluidics **4**, 022811 (2010).
[10] M. Dürr, J. Kentsch, T. Muller, T. Schnelle, and M. Stelzle, Electrophoresis **24**, 722 (2003).
[11] F. Grom, J. Kentsch, T. Muller, T. Schnelle, and M. Stelzle, Electrophoresis **27**, 1386 (2006).
[12] M. Moschallski *et al.*, Electrophoresis **31**, 2655 (2010).
[13] B. H. Lapizco-Encinas and M. Rito-Palomares, Electrophoresis **28**, 4521 (2007).
[14] A. Bonincontro, C. Mari, M. Mengoni, and G. Risuleo, Biophys. Chem. **67**, 43 (1997).
[15] R. Hölzel, NanoBiotechnology **3**, 28 (2009).
[16] A. Henning, F. F. Bier, and R. Holzel, Biomicrofluidics **4**, 022803 (2010).
[17] D. J. Bakewell and H. Morgan, IEEE Trans. Nanobiosci. **5**, 139 (2006).
[18] S. Tuukkanen, A. Kuzyk, J. J. Toppari, H. Hakkinen, V. P. Hytonen, E. Niskanen, M. Rinkio, and P. Torma, Nanotechnology **18**, 295204 (2007).
[19] D. J. Bakewell, I. Ermolina, H. Morgan, J. Milner, and Y. Feldman, Biochim. Biophys. Acta **1493**, 151 (2000).
[20] R. Yokokawa, Y. Manta, M. Namura, Y. Takizawa, N. C. H. Le, and S. Sugiyama, Sens. Actuators B **143**, 769 (2010).
[21] M. L. Du, F. F. Bier, and R. Holzel, AIP Conf. Proc. **859**, 65 (2006).
[22] D. Porschke and J. Antosiewicz, Biophys. J. **58**, 403 (1990).
[23] I. Tinoco and C. Bustamante, J. Mol. Biol. **293**, 271 (1999).
[24] T. Inoue, R. Pethig, T. A. K. Alameen, J. P. H. Burt, and J. A. R. Price, J. Electrost. **21**, 215 (1988).
[25] T. B. Jones, J. Electrost. **6**, 69 (1979).
[26] See supplementary material at http://dx.doi.org/10.1063/1.3604395 for the description of the flow cell fabrication and IDE microfabrication.
[27] E. J. Simon and D. Vanpraag, Proc. Natl. Acad. Sci. U.S.A. **51**, 1151 (1964).
[28] A. Castellanos, A. Ramos, A. Gonzalez, N. G. Green, and H. Morgan, J. Phys. D: Appl. Phys. **36**, 2584 (2003).
[29] S. Suzuki, T. Yamanashi, S. Tazawa, O. Kurosawa, and M. Washizu, IEEE Trans. Ind. Appl. **34**, 75 (1998).
[30] M. M. Yusupov, G. Z. Yusupova, A. Baucom, K. Lieberman, T. N. Earnest, J. H. D. Cate, and H. F. Noller, Science **292**, 883 (2001).
[31] B. Raton, *CRC Handbook of Chemistry and Physics* (CRC, Boca Raton, FL, 1992).
[32] X. B. Wang, R. Pethig, and T. B. Jones, J. Phys. D: Appl. Phys. **25**, 905 (1992).
[33] J. Lyklema, *Fundamentals of Interface and Colloid Science* (Academic, New York, 1995).
[34] I. Ermolina and H. Morgan, J. Colloid Interface Sci. **285**, 419 (2005).

[35]L. F. Zheng, J. P. Brody, and P. J. Burke, Biosens. Bioelectron. **20**, 606 (2004).
[36]I. F. Cheng, S. Senapati, X. G. Cheng, S. Basuray, H. C. Chang, and H. C. Chang, Lab Chip **10**, 828 (2010).
[37]U. Z. Littauer, Biophys. Chem. **86**, 259 (2000).